Int. J. Therm. Sci. (2000) 39, 616–634

S1290-0729(00)00210-6/FLA

Free convection in a vertical cylindrical enclosure

Taoufik Amara [a], Khalifa Slimi [b], Sassi Ben Nasrallah [c*]

[a] *Heat and Mass Transfer Laboratory, National Engineering School, Ibn Eljazzar Street, 5019 Monastir, Tunisia*

[b] *Engineering Preparatory Institute of Monastir, Ibn Eljazzar Street, 5019 Monastir, Tunisia*

[c] *National Engineering High School of Monastir, Ibn Eljazzar Street, 5019 Monastir, Tunisia*

(Received 15 March 1999, accepted 5 October 1999)

Abstract — The problem of transient natural convection which occurs in a vertical cylinder opened at both ends, filled with a fluid saturated porous medium and heated with a periodical lateral heat flux density is outlined. The present study is carried out by the use of the Darcy flow model, and it assumes local thermal equilibrium between the solid and fluid phases. The wall heat conduction is taken into account. Numerical simulations provide us with the evolution of flow and temperature fields within the cylinder. The analysis of flow and thermal field response to any changes in the period of heat pulsation values, the ratio of the wall thermal diffusivity to the porous medium thermal diffusivity and the thickness of the wall are reported in the course of this study. © 2000 Éditions scientifiques et médicales Elsevier SAS

natural convection / vertical cylindrical enclosure / periodical heat flux density / wall heat conduction / numerical simulation / porous medium

Nomenclature

A_i	interior aspect ratio of the cylinder, R_i/H	
A_e	exterior aspect ratio of the cylinder, R_e/H	
Bi	Biot number, hH/λ_p	
$Bi_{i,o}$	modified Biot number, $h_{i,o}H/\lambda_w$	
c_p	specific heat capacity at constant pressure	$J\cdot kg^{-1}\cdot K^{-1}$
e	dimensionless wall thickness, $A_e - A_i$	
Fr	dimensionless heat pulsation frequency	
g	acceleration due to gravity	$m\cdot s^{-2}$
Ra^*	modified Rayleigh number, $kg\beta qH^2/(\alpha_p \upsilon_f \lambda_w)$	
H	cylinder height	m
h, h_o	heat transfer coefficients at the outlet of the cylinder	$W\cdot m^{-2}\cdot K^{-1}$
h_i	heat transfer coefficient at the inlet of the cylinder	$W\cdot m^{-2}\cdot K^{-1}$
k	permeability	m^2
P'	pressure	$kg\cdot m^{-1}\cdot s^{-2}$
P	dimensionless pressure	
P_0	ambient pressure	$kg\cdot m^{-1}\cdot s^{-2}$
q	heat flux density	$W\cdot m^{-2}$
q_0	reference heat flux density	$W\cdot m^{-2}$
q_v	flow rate	$m^3\cdot s^{-1}$
r'	radial coordinate	m
R	cylinder radius	m
R_d	thermal diffusivity ratio, α_w/α_p	
t'	time	s
t	dimensionless time	
T'	temperature	K
T	dimensionless temperature	
T_0	ambient temperature	K
u'_r, u'_z	axial and transverse velocity components	$m\cdot s^{-1}$
u_r, u_z	dimensionless axial and transverse velocity components	
r	dimensionless transverse coordinate	
z'	axial coordinate	m
z	dimensionless axial coordinate	

Greek symbols

α_p	thermal diffusivity of the porous medium, $\alpha_p = \lambda_p/(\rho c_p)_f$	$m^2\cdot s^{-1}$
β	fluid coefficient of volume expansion	K^{-1}
ε	average porosity	
Φ	exchanged heat flux at the cylinder exit	W

* Correspondence and reprints.
Sassi.bennasrallah@enim.rnu.tn

λ	thermal conductivity	$W \cdot m^{-1} \cdot K^{-1}$
γ	volumetric specific heat ratio, $(\rho c_p)_p/(\rho c_p)_f$	
μ_f	fluid's dynamic viscosity	$kg \cdot m^{-1} \cdot s^{-1}$
v_f	fluid's kinematic viscosity	$m^2 \cdot s^{-1}$
Ω	dimensionless heat pulsation period	
ρ_f	fluid's density	$kg \cdot m^{-3}$

Subscripts

c	cold
f	fluid
h	hot
i	inlet
o	outlet
p	porous
r	ratio
ref	reference
ss	steady state
w	wall

Superscripts

$*, '$	dimensionless quantities

1. INTRODUCTION

Natural convection in a open-ended porous medium filled structures is of theoretical importance in recent years. It has also many engineering applications mainly relevant to building insulation, fire protection techniques, heat storage beds, hazardous thermochemical spreading, cooling of electronic components, and so on. One of the principal characteristics of buoyancy induced flows in open-ended systems is their basic geometry which, among other aspects, reveals the interactions and the influence of the inner (inside the medium) and outer (the open region) flow and thermal fields. A theoretical analysis of open-ended structures problems poses the inherent challenge of specifying boundary conditions at the open end (Vafai and Ettefagh [1, 2] and Desai and Vafai [3]).

Transient heat transfer in a fluid saturated porous enclosure caused by a step change in vertical wall temperature was treated by Poulikakos and Bejan [4] with the Darcy law. The analysis was extended later by the same authors [5] for higher Rayleigh number, using the Darcy–Forchheimer model.

The problem of natural convection within a fluid rectangular enclosure subjected to oscillatory temperature at one vertical wall has been studied by Yang et al. [6]. Antohe and Lage [7] investigated theoretically and numerically the evolution of flow and temperature fields within a fluid saturated porous medium enclosure heated periodically from one side wall with the opposite side wall maintained at a constant temperature and the other surfaces insulated.

Although most of the physical systems have a finite wall conductance, only a small number of studies take into account the interaction between convection in the fluid filled porous media and heat conduction in the wall. Bejan and Anderson [8] demonstrated that the insert of a vertical impermeable partition reduces significantly the net heat transfer rate through the porous layer. In addition, Kim and Viskanta [9] showed that the thermal wall conductance could lead to significant changes in the convective heat transfer coefficient for a viscous fluid in an enclosure. However, the studies have neglected the interaction between convection in the fluid-filled porous cavity and conduction of heat in the bounding wall forming the enclosure by using idealised boundary conditions such as those corresponding to a prescribed heat flux or temperature. Chang and Lin [10] have examined the effects of wall heat conduction and anisotropy on natural convection in a fluid-saturated porous medium filled in a rectangular cavity. The authors have used the Darcy flow model and assumed the steady state regime. To the authors knowledge, the problem of transient natural convection in a saturated porous vertical cylindrical enclosure opened at both ends and heated with a periodical lateral heat flux density seems not to have been studied elsewhere. This has motivated the present study.

The present paper deals with unsteady natural convection which occurs in a vertical cylindrical enclosure opened at both ends, filled with a fluid saturated porous medium and heated with a periodic lateral heat flux density. The present study is carried out by the use of the Darcy law and it takes into account heat conduction in the wall. A one-temperature model which supposed the validity of the thermal equilibrium assumption is used for energy transport. The set of equations is resolved numerically by the standard finite volume method as given by Patankar [11]. The numerical simulations provide us with the time–space evolution of flow and temperature fields within the cylinder as well as the analysis of flow and thermal fields response to any changes in the frequency of heat pulsation values, the ratio of the thermal wall diffusivity to the thermal porous medium diffusivity and the wall thickness.

2. FORMULATION OF THE PROBLEM

A schematic of the physical model and coordinate system is given in *figure 1*. The vertical cylinder is opened at both ends, filled with a fluid saturated porous medium and subjected to intermittent heating from the lateral wall. The porous medium is considered to be homogeneous, isotropic, and at local thermal equilibrium. The thermophysical properties of the solid matrix and the fluid are assumed to be constant except in the body force term of the Darcy law invoking the Boussinesq's approximation. Although the porosity varies near the wall (Vafai [12]), the present study assumes constant porosity throughout the cylinder.

The nondimensionalization of the governing equations is carried out on the basis of the following definitions:

$$(r, z) = \frac{(r', z')}{H}, \qquad T = \frac{T' - T_0}{q_0 H/\lambda_w}$$
$$P = \frac{P' - P_0}{\alpha_p \mu_f / k}, \qquad (u_r, u_z) = \frac{(u'_r, u'_z)}{\alpha_p / H} \tag{1}$$
$$t = \frac{t'}{H^2/\alpha_p}, \qquad Q = \frac{q}{q_0}$$

The resulting continuity, Darcy law and energy equations in terms of dimensionless variables are as follows (Ben Nasrallah et al. [13]):

- *Continuity*

$$\frac{1}{r}\frac{\partial (r u_r)}{\partial r} + \frac{\partial u_z}{\partial z} = 0 \tag{2}$$

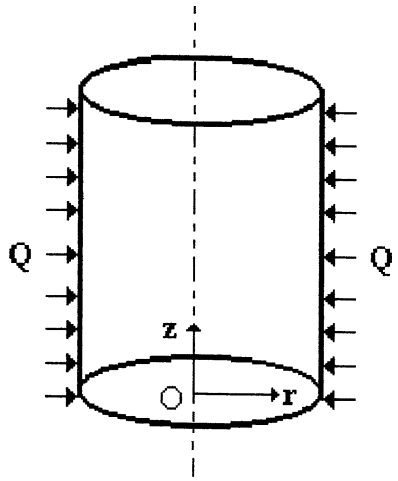

Figure 1. Geometry and coordinate system.

- *Darcy law*

$$u_r = -\frac{\partial P}{\partial r}, \qquad u_z = -\frac{\partial P}{\partial z} + Ra^* T \tag{3}$$

Equations (2) and (3) together yield the so-called "*Poisson's equation*" as

$$\frac{1}{r}\frac{\partial}{\partial r}\left(r\frac{\partial P}{\partial r}\right) + \frac{\partial}{\partial z}\left(\frac{\partial P}{\partial z}\right) = Ra^* \frac{\partial T}{\partial z}$$

- *Energy conservation in the porous medium*

$$\gamma \frac{\partial T}{\partial t} + \left(u_r \frac{\partial T}{\partial r} + u_z \frac{\partial T}{\partial z}\right) = \left\{\frac{1}{r}\frac{\partial}{\partial r}\left(r\frac{\partial T}{\partial r}\right) + \frac{\partial}{\partial z}\left(\frac{\partial T}{\partial z}\right)\right\} \tag{4a}$$

where γ is the volumetric specific heat ratio, $\gamma = (\rho c_p)_p/(\rho c_p)_f$.

- *Energy conservation in the wall*

$$\frac{\partial T_w}{\partial t} = R_d\left\{\frac{1}{r}\frac{\partial}{\partial r}\left(r\frac{\partial T_w}{\partial r}\right) + \frac{\partial}{\partial z}\left(\frac{\partial T_w}{\partial z}\right)\right\} \tag{4b}$$

where the subscript w means a wall quatity and R_d is the ratio of the wall thermal diffusivity to that of the porous medium, $R_d = \alpha_w/\alpha_p$.

2.1. Initial and boundary hydrodynamic conditions

$$P(r, z, 0) = 0 \quad \text{at } t \le 0 \tag{5}$$

The boundary condition on the pressure at the inlet of the cylinder is written as (Bernoulli's law):

$$P'(r', 0, t') = P_0 - \frac{1}{2}\rho_0 U'^2$$

U' being the velocity at the entrance of the cylinder and P_0 the atmospheric motorise pressure. Dalbert et al. [14] have studied the influence of the term $-\frac{1}{2}\rho_0 U'^2$ on fluid flow by natural convection of a Newtonian fluid in a vertical channel heated by a constant heat flux. They have shown that this correction of the motorise pressure enhanced results only for considerable heating rates. In our case, we consider a fluid flow through a porous medium where the velocity remains very weak. Then, we can neglect the effect of the term $-\frac{1}{2}\rho U'^2$:

$$P(r, 0, t) = P(r, 1, t) = 0 \quad \text{for } 0 < r < A_i \tag{6}$$

The bounding wall $r' = R_i$ is supposed impermeable and as a result the boundary hydrodynamic condition required at this level is of the type

$$\left.\frac{\partial P'}{\partial r'}\right|_{r'=R_i} = 0 \tag{7}$$

which follows directly from the Darcy law by writing $u'_r|_{r'=R_i} = 0$:

$$\frac{\partial P}{\partial r}(0, z, t) = \frac{\partial P}{\partial r}(A_i, z, t) = 0 \tag{8}$$

2.2. Initial and boundary thermal conditions

$$T(r, z, 0) = T_w(r, z, 0) = 0 \quad \text{at } t \le 0 \tag{9}$$

The thermal boundary condition at the inlet of the cylinder can be written as $T' = T_0$. Indeed, in a cheminey flow, a thermal boundary layer will be developed in the cylinder. The thickness of this thermal boundary layer is negligible at the entrance region of the medium. Thereby, the temperature at this region remains equal to the temperature of the surrounding, in occurrence T_0.

We have also undertaken a sensitivity study to the thermal boundary condition on the temperature, by taking a thermal boundary condition of the type

$$-\lambda_p \left.\frac{\partial T}{\partial z'}\right|_{z'=0} = h\left(T' - T_0\right)$$

This study has shown that the temperature at the entrance is insensitive to the choice of the heat transfer coefficient h and it remains equal to the temperature of the surrounding. So, at the inlet we have:

$$T(r, 0, \tau) = 0 \quad \text{for } 0 < r < A_i \tag{10a}$$

At the bottom of the heated wall, the thermal boundary condition is expressed as

$$\frac{\partial T_w}{\partial z}(r, 0, t) = Bi_i T_w(r, 0, t) \quad \text{for } A_i < r < A_e \tag{10b}$$

Owing to the revolution symmetry at $r = 0$, we have:

$$\frac{\partial T}{\partial r}(0, z, t) = 0 \tag{11}$$

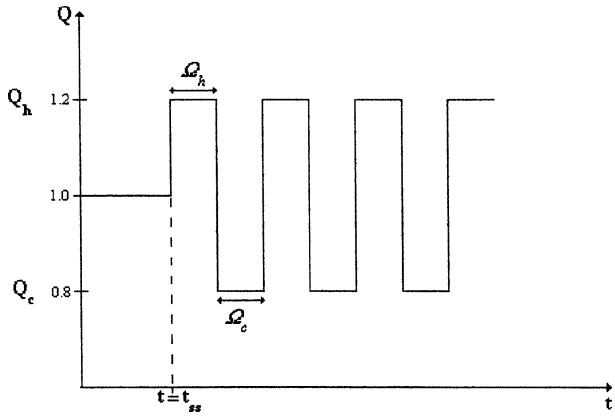

Figure 2. Periodical heat flux density.

At the lateral wall, a periodical heat flux density was applied (*figure 2*):

$$\frac{\partial T_w}{\partial r}(A_e, z, t) = Q(t) \tag{12a}$$

The temperature continuity $r = A_i$ is introduced by the following equation:

$$T(A_i, z, t) = T_w(A_i, z, t) \tag{12b}$$

At the cylinder exit, the existent flow upper the porous surface is very complicated. On one hand, the upper face releases a natural convection fluid flow similar to that observed over a heated horizontal flat plate. On the other hand, the outlet fluid flow disturbs the effect of the heated horizontal flat plate and, under certain conditions, it can allow fluid to re-enter the cylinder as a recirculatory flow. To avoid this problem, we are expected to make larger the calculating domain in order to take into account the fluid flow and heat transfer near the outlet face, which will complicate the study. To avoid this problem, we introduce in the case of an upward flow ($u_z > 0$), a heat transfer coefficient as (Slimi et al. [15])

$$-\frac{\partial T}{\partial z}(r, 1, t) = Bi\, T(r, 1, t) \quad \text{if } u_z > 0 \quad \text{for } 0 < r < A_i \tag{13a}$$

In the case of a downward flow ($u_z < 0$), the boundary condition at the exit of the cylinder is

$$T(r, 1, t) = 0 \quad \text{if } u_z < 0 \quad \text{for } 0 < r < A_i \tag{13b}$$

At the superior face of the wall, the boundary condition is expressed as follows:

$$-\frac{\partial T}{\partial z}(r, 1, t) = Bi_o T_w(r, 1, t) \quad \text{for } A_i < r < A_e \tag{13c}$$

3. NUMERICAL PROCEDURE

The governing equations are solved by the standard finite volume method (Patankar [11]), which is based on the solution of difference equations obtained by integrating the differential equations for continuity, momentum and energy over control volume enclosing the nodal points. The advantage of this method is to insure the flux conservation.

In the present study, we have used a uniform grid in the porous medium and a fine and uniform grid in the wall (*figure 3*).

In order to ensure the stability of the numerical model, the convective terms are discretized using the upwind scheme. A fully implicit scheme is used for the temporal terms.

By first assuming a temperature distribution within the entire medium, the Poisson's equation is solved by line-by-line iteration giving the pressure distribution in the cylinder. Then the set r- and z-velocity are determined and energy equations for the porous medium and the wall are solved also by line-by-line iteration. After a sweep of the solution domain is completed, numerical convergence is examined locally following the criterion

$$\mathrm{MAX}\left|\frac{\phi_{n,m}^{i+1}-\phi_{n,m}^{i}}{\phi_{n,m}^{i}}\right| < \varepsilon \qquad (14)$$

where ϕ is replaced by P and T at every (m,n) location of the discretized domain, i and $i+1$ are two consecutive iterations at the same time τ, and ε is a given tolerance.

To examine the validity of the numerical scheme, our numerical results, for the velocity and temperature distributions, were compared with the numerical results obtained by Ben Nasrallah et al. [13] by making the necessary changes. They all agree at least up to three decimal places. The comparison is not shown here for the sake of brevity.

To check again the accuracy of our results comparison is also made with previous published results related to steady free convection in a vertical annulus filled with a saturated porous medium and whose vertical walls are at constant temperatures, the horizontal walls being insulated (Hickox and Gartling [16] and Prasad and Kulacki [17]).

Tables I and *II* show good agreement between our numerical results and those obtained in previous published results.

In *tables I* and *II*, A and κ are, respectively, the aspect ratio, $A = H/(r_e - r_i)$, and the radius ratio of the cylindrical annulus, $\kappa = r_e/r_i$, and *Ra* is the Rayleigh number defined as in Hickox and Gartling [16] and Prasad and Kulacki [17].

Our numerical results for Nusselt number are also compared with the experimental results of Prasad [18] and the numerical ones of David et al. [19] (*table III*).

Here, in *table III*, $\vartheta = d/(r_e - r_i)$ is the ratio of the solid diameter and the annulus width, Pr_f is the fluid

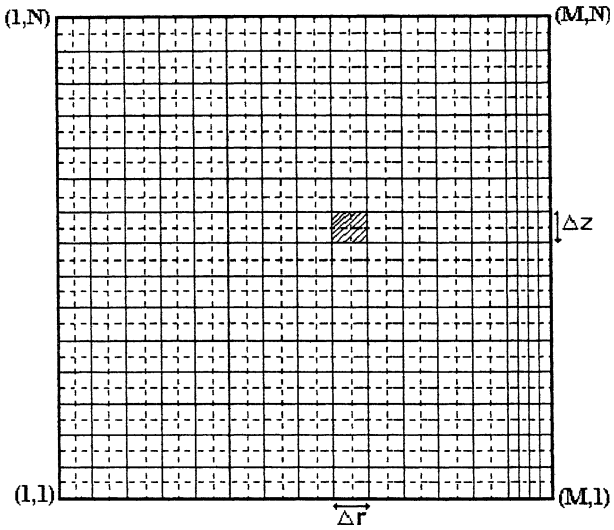

Figure 3. Discretized domain.

TABLE I
Comparison of present values of average Nusselt number with the values obtained in previous published results.

	$A=2$			$A=4$			$A=6$			$A=8$		
κ	2	3	5	1.5	2	3	1.33	1.67	2.33	1.25	1.5	2
Hickox and Gartling [16]	4.190	4.741	5.590	2.879	3.216	3.750	2.277	2.506	2.886	1.951	2.117	2.409
Prasad and Kulacki [17]	4.048	4.738	5.716	2.751	3.123	3.692	2.172	2.412	2.806	1.862	2.033	2.327
Present results	4.012	4.535	5.419	2.888	3.292	3.800	2.379	2.615	2.982	2.063	2.234	2.520

TABLE II
Comparison of present values of average Nusselt number with the values obtained in previous published results.

	$\kappa = 2$				$\kappa = 5$				$\kappa = 10$			
Ra	75	50	50	50	120	120	80	80	135	135	90	90
A	1	1	10	20	2.5	6.25	2.5	12.5	2.222	5.555	2.222	11.11
Prasad and Kulacki [17]	3.59	2.77	1.72	1.57	5.79	4.15	4.83	2.99	8.17	6.05	6.88	4.54
Present results	3.60	2.89	1.86	1.68	5.45	4.11	4.60	3.03	7.44	5.83	6.39	4.45

TABLE III
Comparison of present values of average Nusselt number with experimental and numerical ones for $\kappa = 5.338$, $A = 1$.

d (mm)	ϑ	Pr_f	Ra_f	Prasad [18]	David et al. [19]	Present results
3	0.0242	5.46	$6.50{\cdot}10^8$	9.058	8.984	8.971
		4.51	$1.90{\cdot}10^9$	21.15	16.12	16.07
		4.11	$3.03{\cdot}10^9$	26.77	21.00	20.95
6	0.0484	6.17	$1.42{\cdot}10^8$	10.44	9.169	9.17
		5.72	$3.61{\cdot}10^8$	19.86	15.71	15.72
		4.98	$1.12{\cdot}10^9$	39.53	29.76	29.78
		4.37	$2.38{\cdot}10^9$	58.11	44.84	44.86
22.25	0.1796	6.01	$4.67{\cdot}10^7$	23.46	25.98	25.96
		5.86	$1.46{\cdot}10^8$	37.10	56.48	56.44
		5.65	$2.75{\cdot}10^8$	51.06	66.84	66.80
		5.46	$4.32{\cdot}10^8$	59.56	79.48	79.45

Prandtl number, $Pr_f = \nu_f/\alpha_f$, and Ra_f is the Rayleigh number of the fluid,

$$Ra_f = \frac{g\beta(r_e - r_i)^3 \Delta T}{\alpha_f \nu_f}$$

The examination of *table III* shows reasonable variations between our numerical results and the experimental ones especially at lower values of ϑ and Ra_f.

4. RESULTS AND DISCUSSION

To help understand the thermal convective effect of wall conductance and of pulsating heat, four physical quantities are chosen: the temperature, pressure, dimensionless flow rate q_v^* and heat flux Φ^* exchanged at the cylinder exit. q_v^* and Φ^* are obtained with integration over the whole section at the cylinder exit and rended dimensionless by employing the following scales:

$$q_{vref} = \frac{\pi R_i^2 \alpha_p}{H}, \qquad \Phi_{ref} = 2\pi R_i H q_0 \qquad (15)$$

In a dimensionless form, q_v^* and Φ^* are written as follows:

$$q_v^* = \frac{2}{A_i^2} \int_0^{A_i} u_z r \, dr \qquad (16)$$

$$\Phi^* = \frac{1}{A_i} \left[\frac{\lambda_p}{\lambda_w} \left(\int_0^{A_i} u_z T r \, dr + Bi \int_0^{A_i} T r \, dr \right) + Bi_o \int_{A_i}^{A_e} T_w r \, dr \right] \qquad (17a)$$

If the heat exchanged by wall end at the cylinder outlet is neglected then the heat flux exchanged at the cylinder exit will be expressed as

$$\Phi^* = \frac{1}{A_i} \frac{\lambda_p}{\lambda_w} \left(\int_0^{A_i} u_z T r \, dr + Bi \int_0^{A_i} T r \, dr \right) \qquad (17b)$$

These two quantities have been chosen for two principal reasons. First, because their representations may help the conception of several industrial applications especially where it is necessary to have an idea on the amount of heat that can be recaptured at the exit of the porous bed

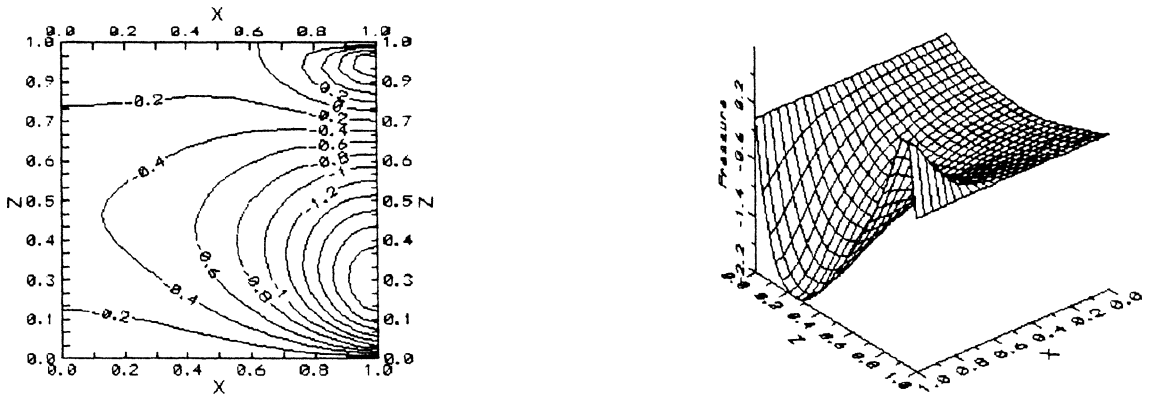

(a)

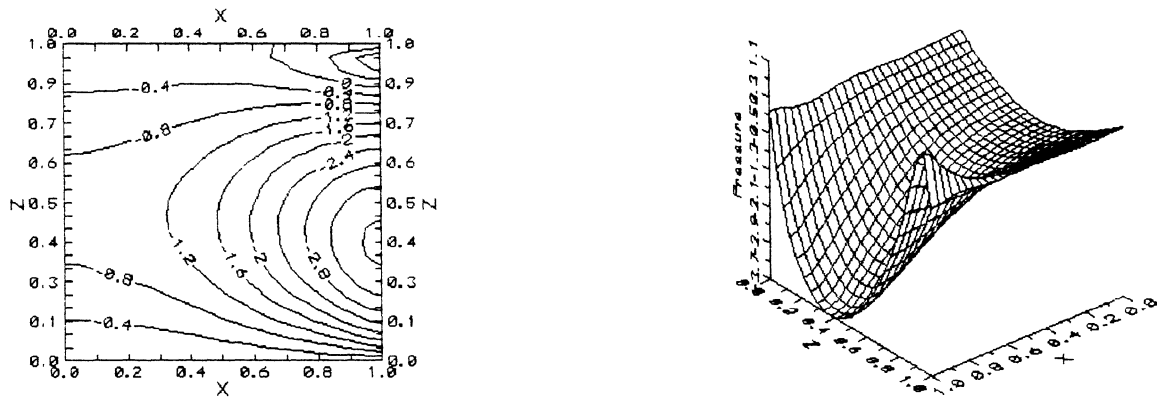

(b)

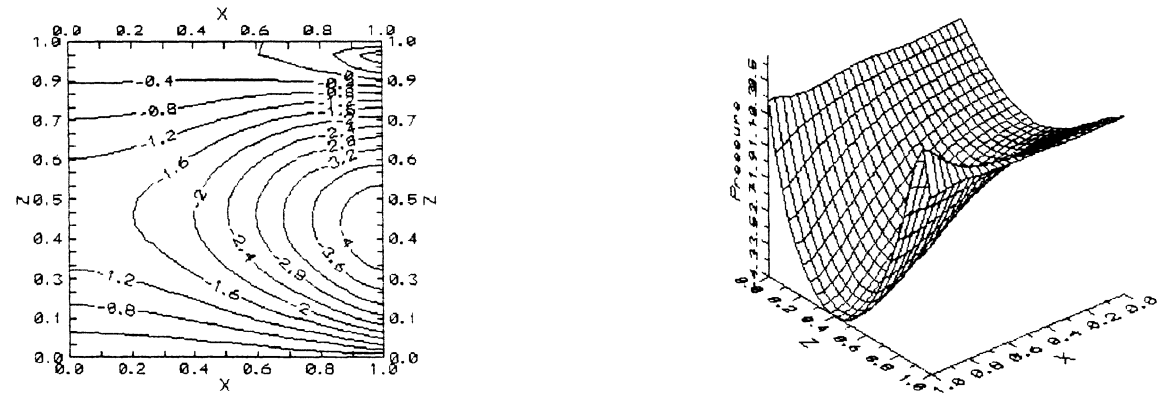

(c)

Figure 4. Time–space evolution of pressure field for (a) $t = 0.03$, (b) $t = 0.05$ and (c) $t = 1$.

and/or the flow rate that can leave this region. Second, because their representations may be useful to distinguish easily the effect of different parameters.

The porous medium enclosed in the vertical cylinder is saturated initially with motionless and isothermal fluid. The first phase of the thermal process refers to the heating of the enclosed quiescent fluid until a steady convection regime is attained. During this phase, a constant dimensionless heat flux $Q = 1$ is imposed at the lateral wall. At $t = t_{ss}$ (which corresponds to the moment when the system reaches steady state, $t' = t'_{ss}$), the system undergoes a second phase during which the input heat fluxes pulsates in time around its reference value.

Here, the heat pulsation half-amplitude is kept at 20 % of the reference value. Equal heating and cooling periods are assumed, $\Omega_h = \Omega_c = \Omega$, so the nondimensional heat pulsation frequency is $Fr = 1/(2\Omega)$.

4.1. Physical phenomena description for a constant prescribed heat flux (first phase)

In this section, all the calculations have been performed for Biot numbers representing the external change, $Bi = 2{\cdot}10^3$, $Bi_i = 10^2$, $Bi_o = 2{\cdot}10^2$, a heat capacity ratio $\gamma = 1.546$, a modified Rayleigh number $Ra^* = 2{\cdot}10^3$, an interior aspect ratio of the cylinder $A_i = 1$, a ratio of the thermal wall diffusivity to the thermal porous medium diffusivity $R_d = 0.1$ and for a constant dimensionless heat flux density $Q = 1$. We have chosen to take $Ra = 2{\cdot}10^3$ and $A_i = 1$ so as to have a flow with top aspiration from the upper porous surface of the cylinder. It has been shown that this type of flow is found for high aspect ratio A and/or great values of the modified Rayleigh number (Ben Nasrallah et al. [13]). It has been demonstrated in a previous work (Slimi et al. [15]) that at this level of modified Rayleigh number (which corresponds to a fluid Grashof number $Gr_f = 2{\cdot}10^8$ in [15]), the Darcy flow model remains valid if the Darcy number $Da = k/H^2$ is lower than 10^{-4}. However, it has been shown that for $Ra^* = 2{\cdot}10^3$, the longitudinal flow is dominant.

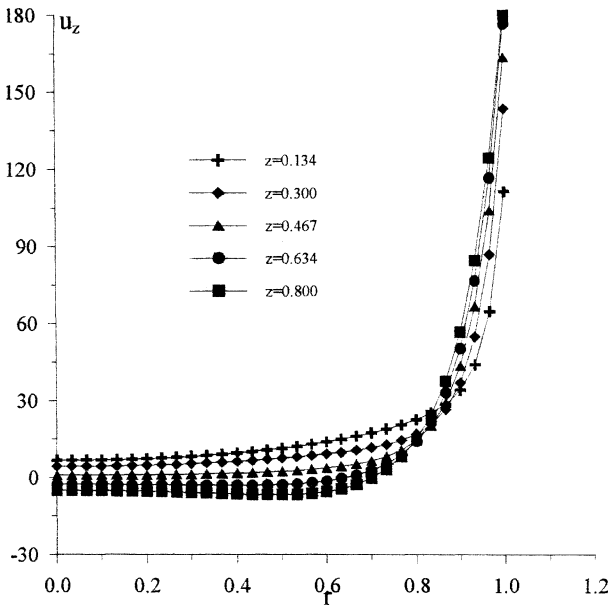

Figure 5. Axial velocity versus radial distance during the first phase of the thermal process.

Figure 4 depicts the time–space variations of pressure within the cylinder. As can be seen, the pressure decreases from the inlet, attains a minimum value and increases, reaches a maximum and decreases to attain the ambient pressure.

The pressure decreases at first with time and, for enough period of time, it tends to be independent of time.

Figure 5 shows the z-component of the velocity field versus radial distance, at different axial locations, during the first phase of the thermal process. As illustrated by this figure, the axial velocity is important in a region close to the heated wall and decreases with the radial distance r.

Figure 6 indicates the time–space variations of the temperature within the cylinder. The isotherms have the same profile found in the case of a heated flat plate in a semi-infinite medium and are confined in the region near the heated wall.

At the cylinder exit, the vertical temperature gradients are high because of the heat loss to surrounding. However, the influence region of these thermal gradients is very scanty.

Figure 7(a) gives, in the steady state, the temperature profile in the entire medium (wall + porous medium) versus radial distance r. Due to the applied lateral heat flux density, the temperature is found to be important in a region close to the heated wall, and it decreases with a decrease of r. As shown in *figure 7(b)*, the temperature in the wall is found to be increased from the inlet of the cylinder attains a maximum and decreases to reach a lower value at the exit due to the heat loss with the surrounding.

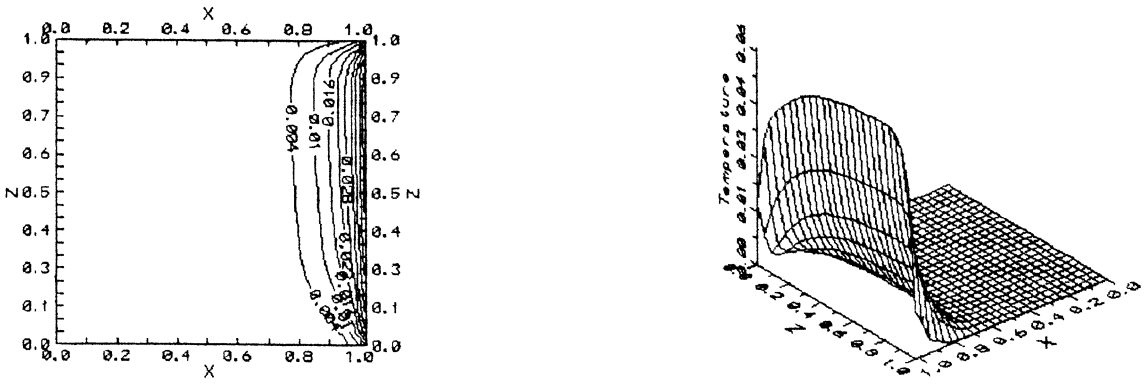

(a)

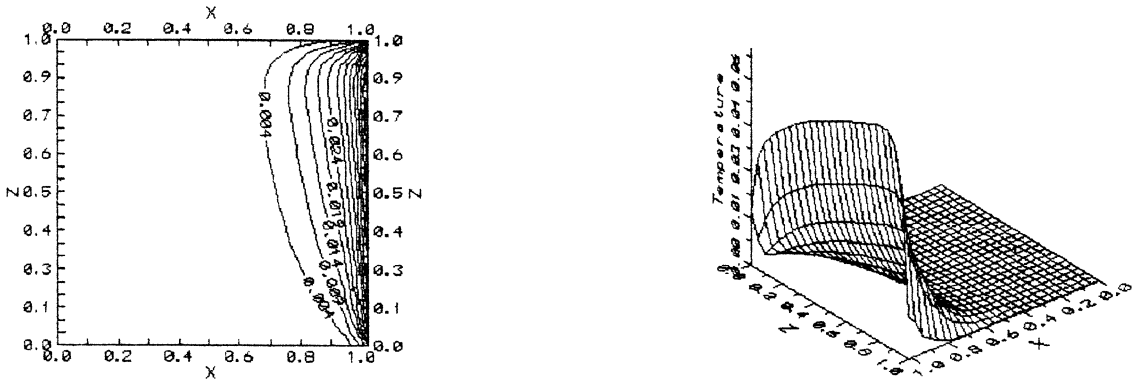

(b)

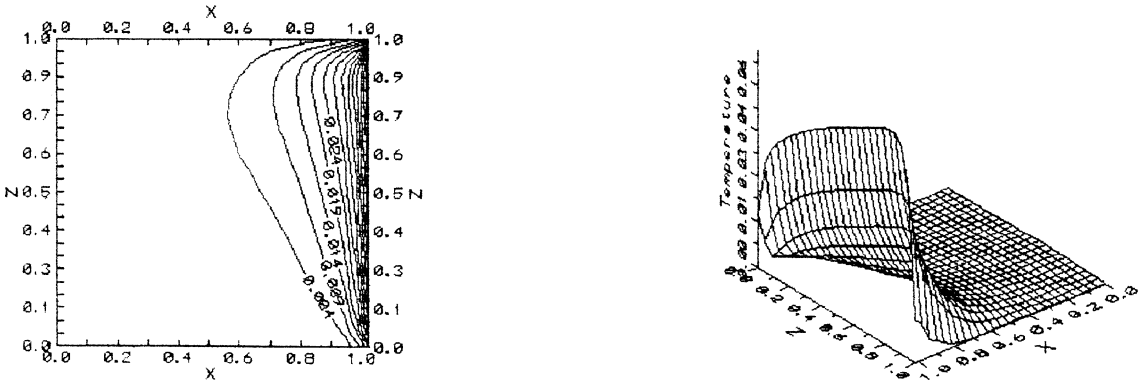

(c)

Figure 6. Time–space evolution of temperature for (a) $t = 0.03$, (b) $t = 0.05$ and (c) $t = 1$.

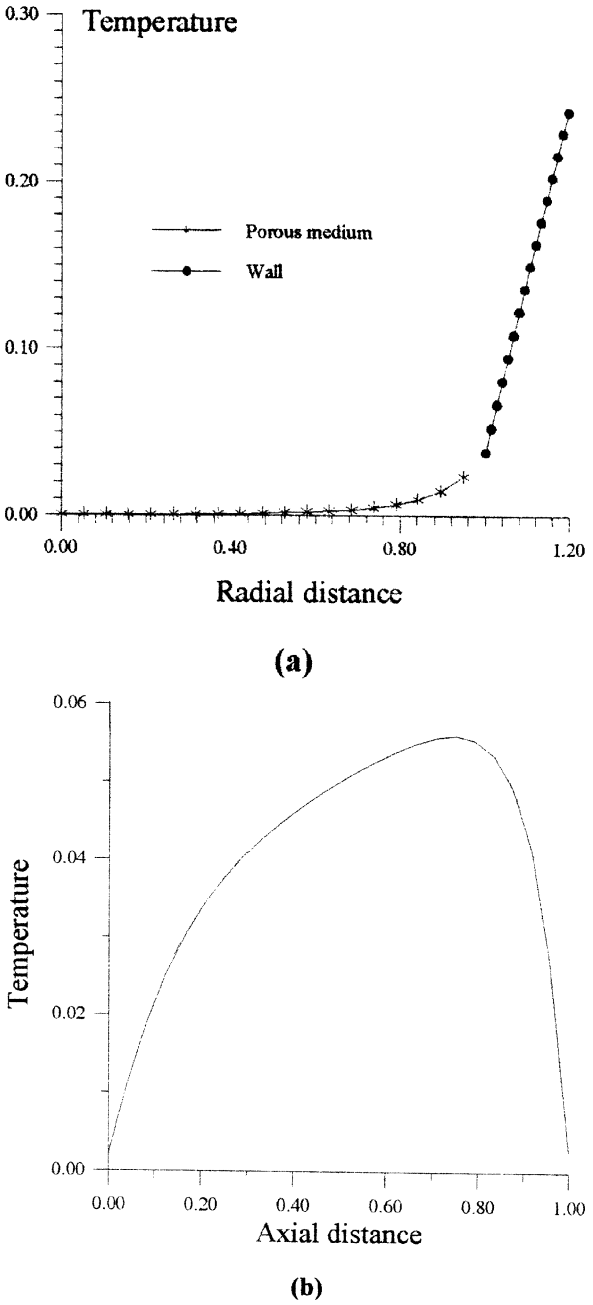

Figure 7. (a) Temperature profile versus radial distance in the entire medium (wall + porous medium). (b) Wall temperature versus axial distance for $r = A_i$ (in the steady state regime).

4.2. Parametric study

4.2.1. Effect of thermal diffusivity ratio

The computations have been carried out for an aspect ratio $A_i = 1$, Biot numbers $Bi = 2{\cdot}10^3$, $Bi_i = 10^2$, $Bi_o =$

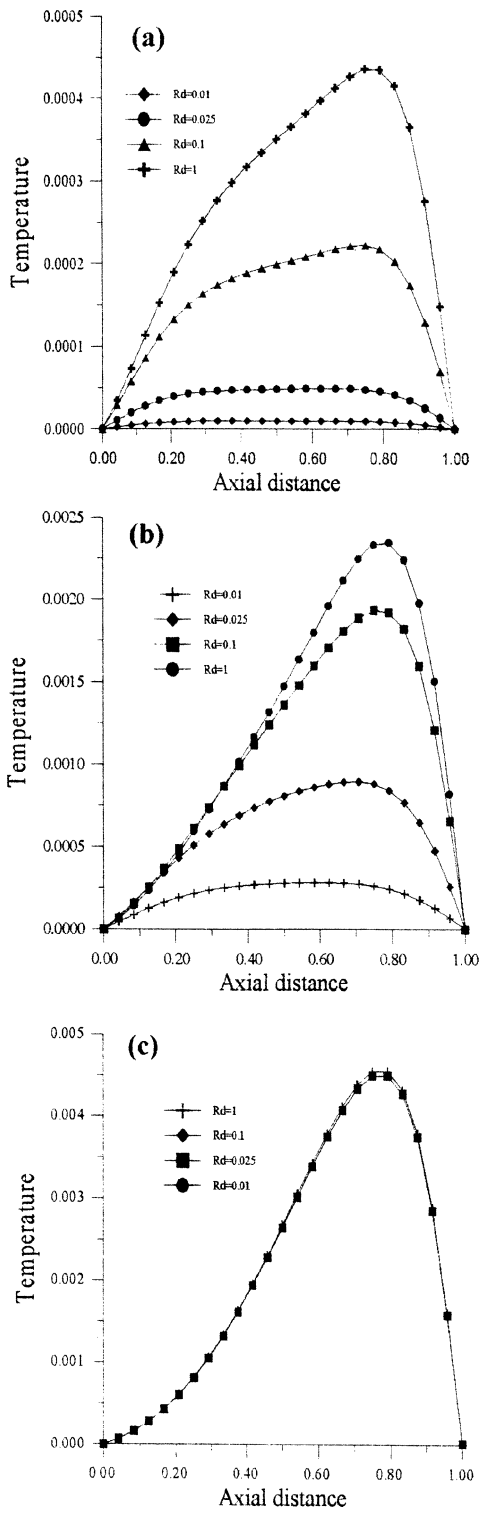

Figure 8. Temperature versus z for $r = 0.58$, for different thermal diffusivity ratio and at (a) $t = 0.03$, (b) $t = 0.005$ and (c) $t = 0.3$.

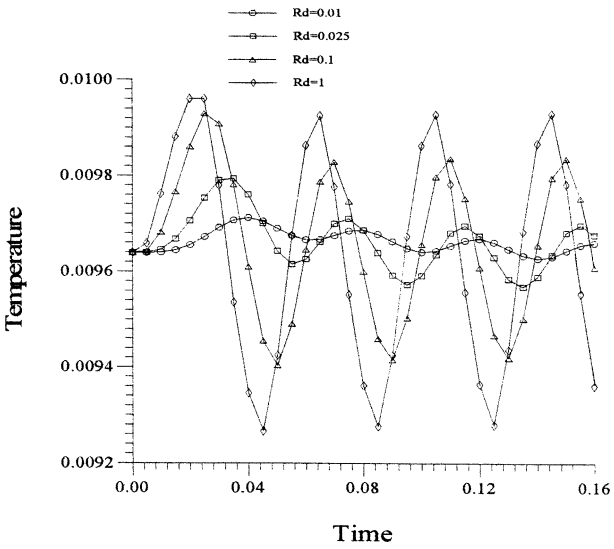

Figure 9. Temperature versus time for $r = 0.8$, $Fr = 25$ and for different values of R_d.

$2{\cdot}10^2$, a wall thickness $e = 0.02$, a modified Rayleigh number $Ra^* = 2{\cdot}10^3$ and for different thermal diffusivity ratio R_d ranging from 0.01 to 1.

The time-evolution of thermal and pressure fields are presented in *figures 8–11* for different values of R_d versus axial distance.

For constant wall heat flux density, it is seen that, in the transient period, the temperature in the porous medium increases with increasing R_d (*figure 8*). In the steady state regime (*figure 8(c)*), the thermal field is insensitive to any change in the value of R_d.

In *figure 9*, we have represented the time-variations of the temperature within the cylinder for a periodical heat flux with a frequency $Fr = 25$ and for different values of R_d. As could be expected, any increase in the value of R_d yields an increase in the amplitude of time-variations of temperature. It can also be concluded from this figure that the maximum of temperature is reached as rapidly as R_d is higher.

We have represented also the time–space variations of pressure within the cylinder for different values of R_d (*figure 10*). It is seen that any increase in the value of R_d is accompanied, in the transient period (*figures 10(a, b)*), by a decrease in the pressure values. *Figure 10(c)* shows that, in the steady state regime, the pressure is insensitive to any change in the value of R_d.

The effect of R_d on the pressure field, in the case of a periodical heat flux, has also been studied (*figure 11*). As expected, the amplitude of time-variations of the pressure increases with the increase of R_d. As the thermal field,

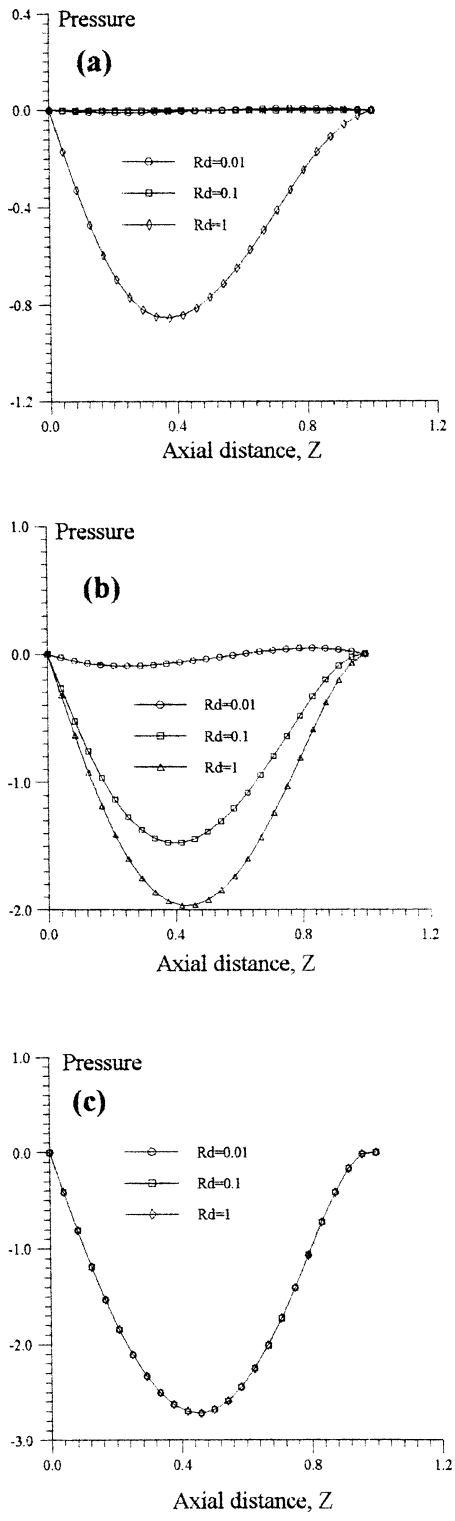

Figure 10. Pressure versus z for $r = 0.6$ and for different thermal diffusivity ratios and at (a) $t = 0.03$, (b) $t = 0.05$ and (c) $t = 1$.

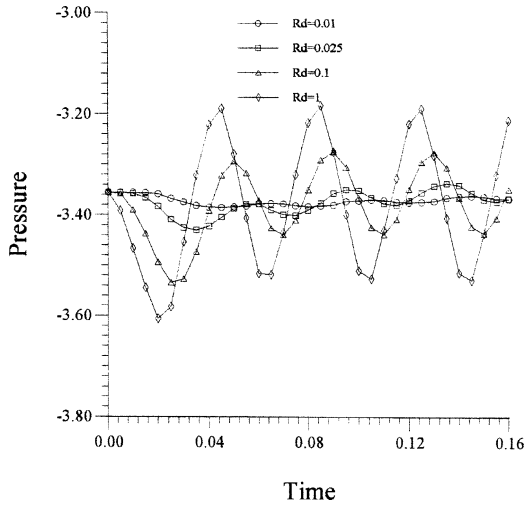

Figure 11. Pressure versus time for $Fr = 25$, $r = 0.77$, $z = 0.58$ and for different values of R_d.

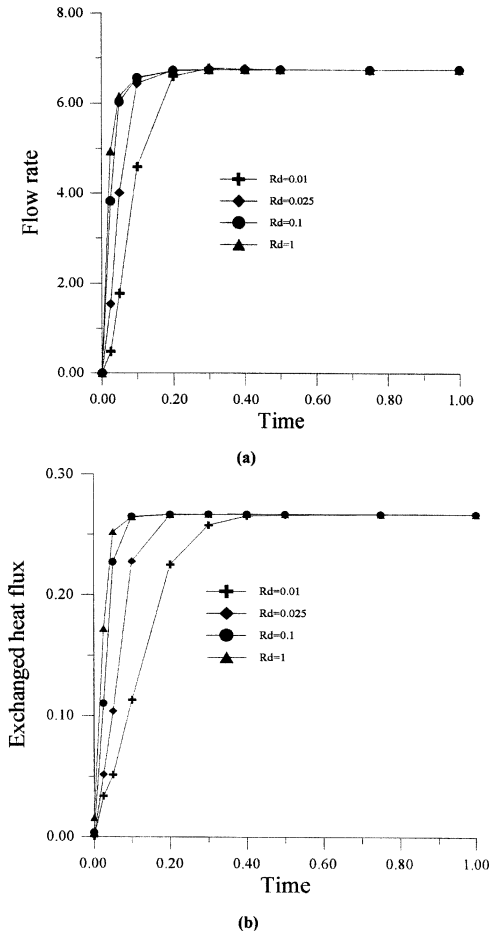

Figure 12. q_v^* and Φ^* versus time for a constant heat flux and for different values of R_d.

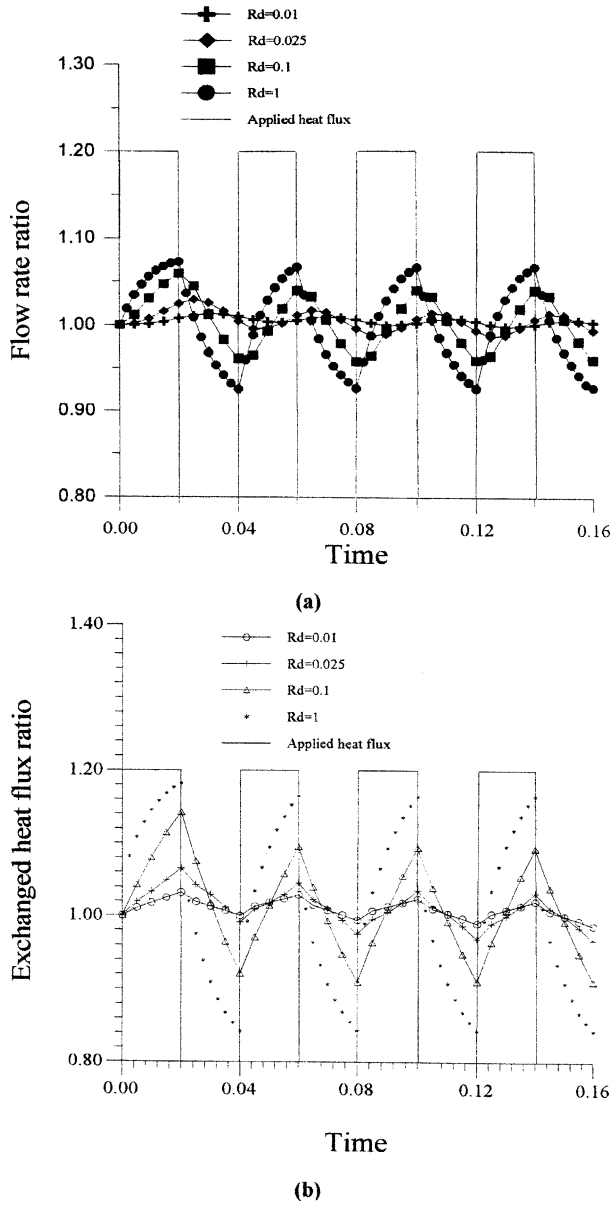

Figure 13. q_{vl}^* and Φ_r^* versus time for a periodical heat flux and for different R_d.

the maximum of the time-variations of the pressure field is found to be attained as rapidly as R_d is higher.

The time-variations of flow rate and heat flux exchanged at the exit of the cylinder are plotted in *figures 12* and *13*.

In the case of a constant wall heat flux density (*figures 12(a, b)*) the steady state regime is reached as rapidly as R_d is important. This is evident because a higher value of R_d corresponds, for a fixed value of the

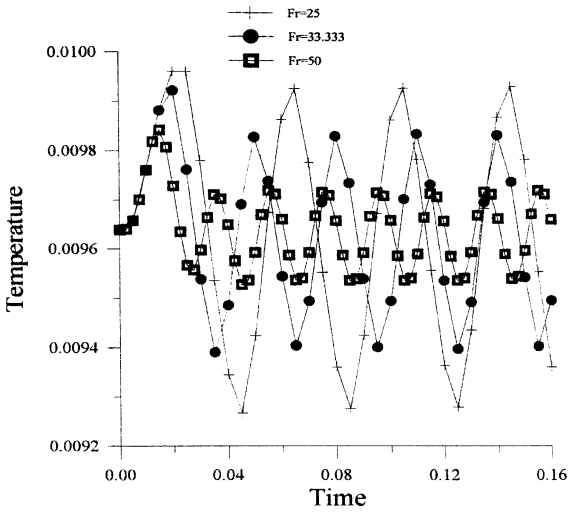

Figure 14. Temperature versus time for $R_d = 1$, $z = 0.58$, $Fr = 33.33$ and (a) for $r = 0.58$ and different Fr and (b) for different r values.

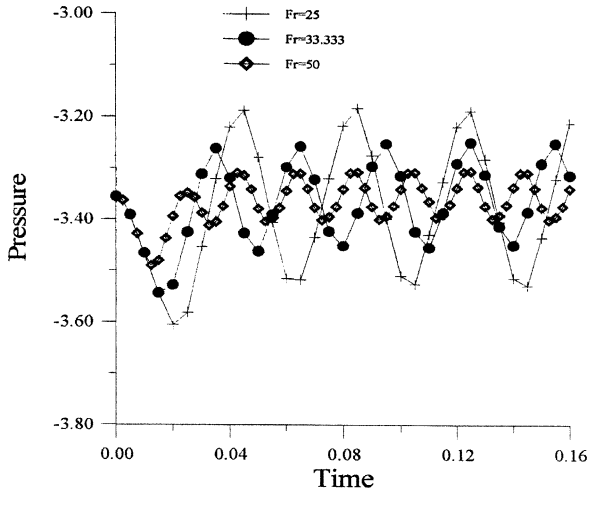

Figure 15. Pressure versus time for $R_d = 1$, $z = 0.58$, $r = 0.78$, $Fr = 25$ and (a) for different Fr values and (b) for different r values.

thermal diffusivity of the porous medium, to a higher wall diffusivity and, consequently, to a less wall inertia and/or a higher wall conductivity.

In the case of a periodical wall heat flux density, we have represented a flow rate ratio and a heat flux ratio as follows:

$$q^*_{vr} = \frac{q^*_v(t > t_{ss})}{q^*_v(t = t_{ss})}, \qquad \Phi^*_r = \frac{\Phi^*(t > t_{ss})}{\Phi^*(t = t_{ss})}$$

We have considered these two parameters in order to distinguish easily the effect of the parameters in the case of a periodical wall heat flux density.

As can be seen from *figures 13(a, b)*, the amplitudes of time-variation of flow rate ratio and of the heat flux ratio increase with R_d. The maximum values of these plots are found to be reached as rapidly as R_d is higher.

4.2.2. Effect of the pulsating heat frequency

To study the effect of the pulsating heat flux frequency, numerical calculations were made with a wall thickness $e = 0.02$, a Rayleigh number $Ra^* = 2{\cdot}10^3$, an interior aspect ratio $A_i = 1$, Biot numbers $Bi = 2{\cdot}10^3$, $Bi_i = 10^2$,

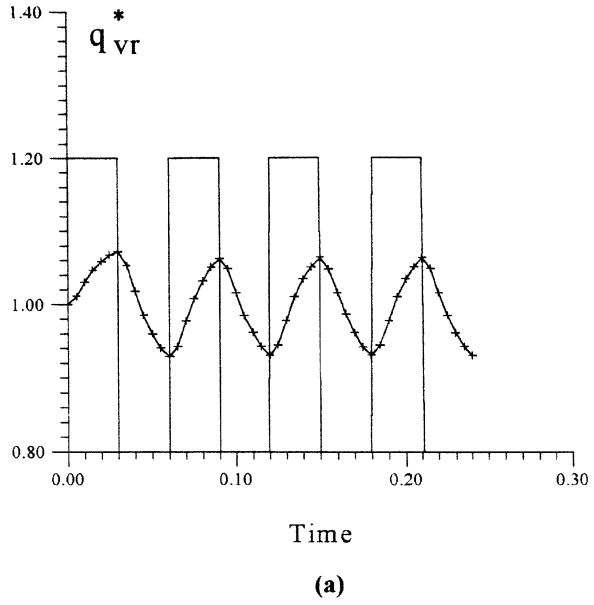

Figure 16. Time-variations of (a) q^*_{vr} and (b) Φ^*_r for $R_d = 0.1$ and $Fr = 16$.

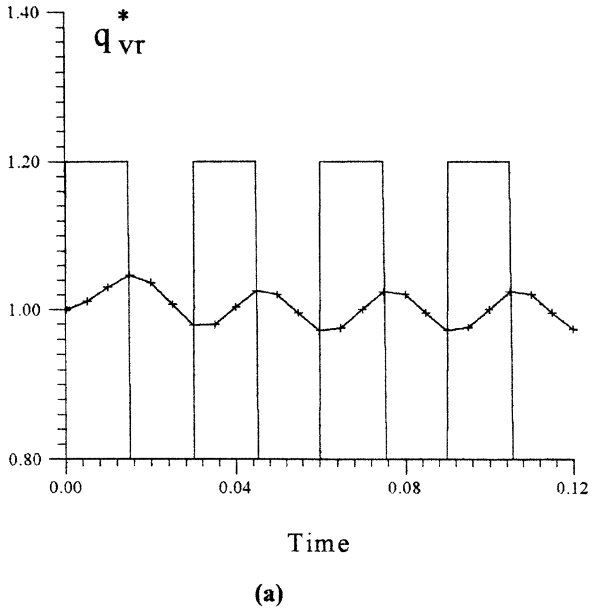

Figure 17. Time-variations of (a) q^*_{vr} and (b) Φ^*_r for $R_d = 0.1$ and $Fr = 33.333$.

$Bi_o = 2{\cdot}10^2$, a diffusivity ratio $R_d = 1$ and for different values of the frequency Fr.

To help understand the effect of the applied heat flux frequency on thermal field, we have chosen the following variable named temperature ratio defined as

$$T_r = \frac{T(t > t_{ss})}{T(t = t_{ss})}$$

As can be seen from *figure 14*, the amplitude of time-variations of the temperature ratio is found to be increased with a decrease in the frequency value. *Figure 14(b)* indicates, for a fixed value of the heat pulsation frequency, a decrease in the amplitude of the temperature ratio far from the heated wall.

In *figure 15(a)*, we have been concerned by the time-variations of the pressure field within the porous medium

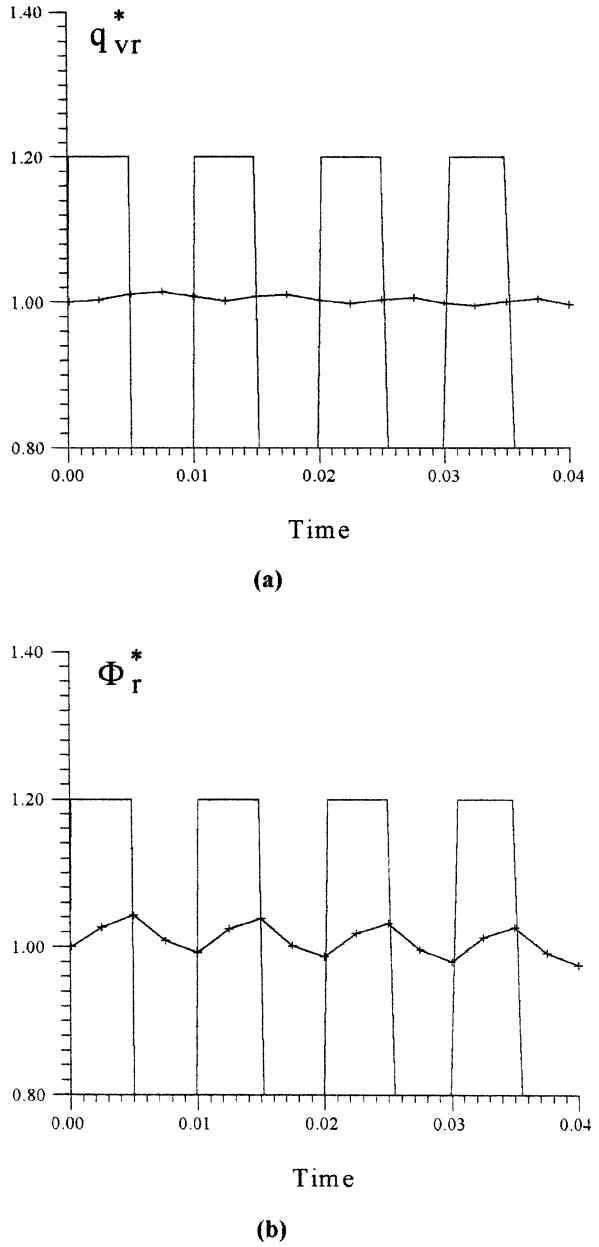

Figure 18. Time-variations of (a) q^*_{vr} and (b) Φ^*_r for $R_d = 0.1$ and $Fr = 100$.

with the heat pulsation frequency. It is found that an increase in the value of *Fr* leads to a decrease in the amplitude of time-variations of the pressure field within the medium. *Figure 15(b)* shows that the amplitude of time-variations of the pressure field is lessened far from the heated wall.

As shown in *figures 16–18*, the amplitude of time-variations of the flow rate ratio q^*_{rv}, and the ratio of heat

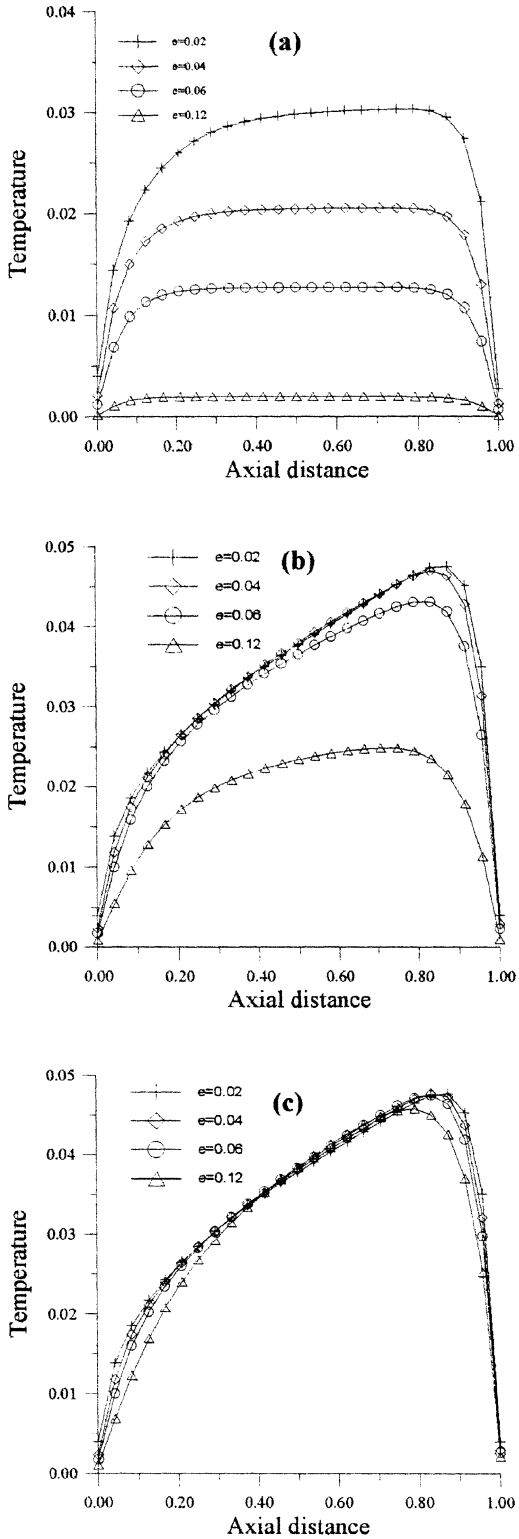

Figure 19. Temperature versus z for $R_d = 1$, $r = A_i$ and at (a) $t = 0.025$, (b) $t = 0.1$ and (c) $t = 0.5$.

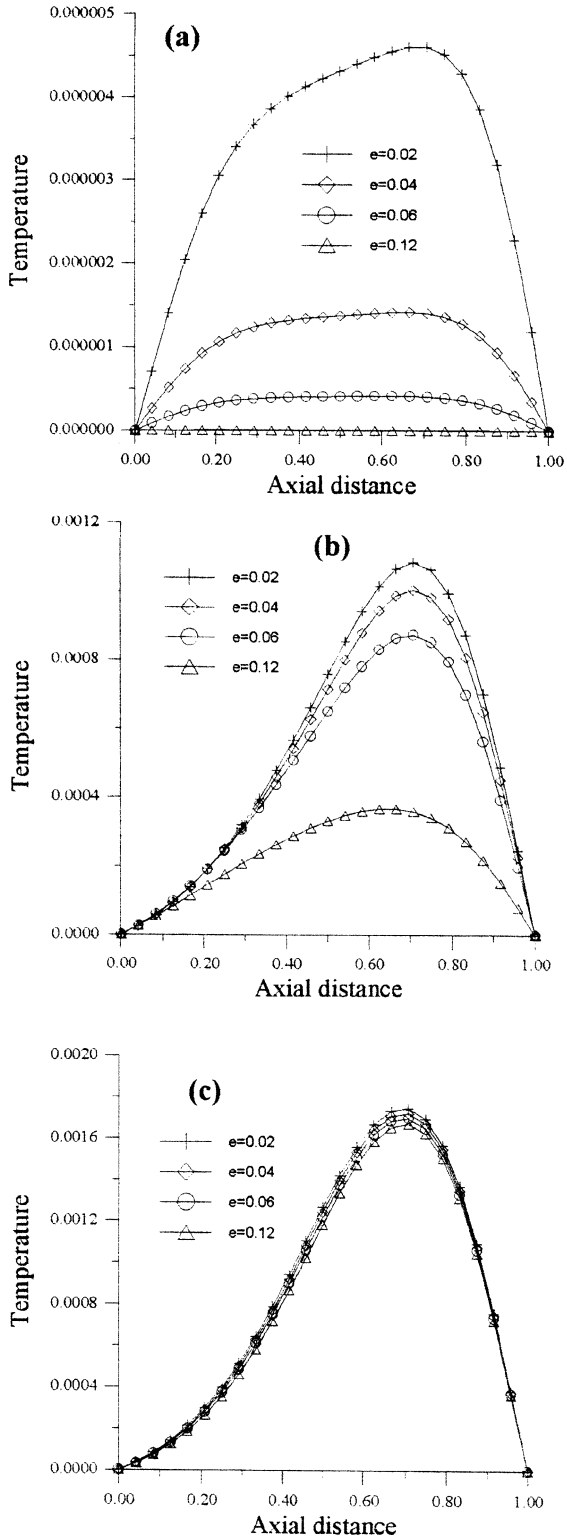

Figure 20. Temperature versus z for $R_d = 1$, $r = 0.37$ and at (a) $t = 0.025$, (b) $t = 0.1$ and (c) $t = 0.5$.

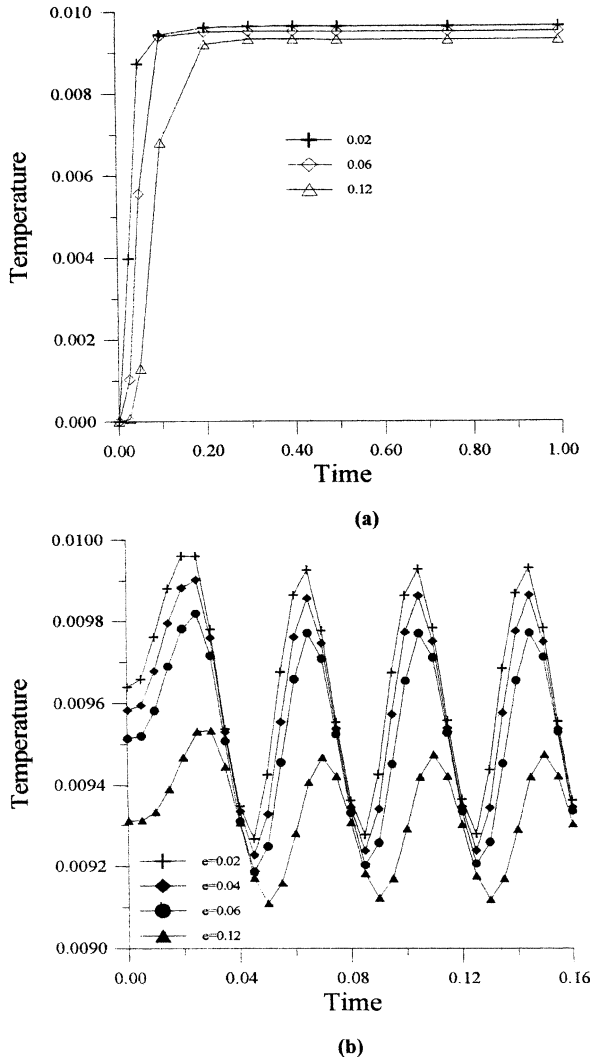

Figure 21. Time-variations of temperature for $r = 0.79$, $z = 0.57$, $Fr = 25$, $R_d = 1$ and (a) a constant heat flux and (b) a periodical heat flux.

flux exchanged at the cylinder exit Φ_r^* is reduced as the frequency is increased. We have also demonstrated that for all modified Rayleigh number values ranging from $3{\cdot}10^2$ to $2{\cdot}10^3$, the system responds to an increase in heat pulsating frequency in a similar fashion. These results, not shown here for the sake of brevity, indicate also that the system is not susceptible to resonance phenomena and an increase in the frequency results in a monotonic decrease in the amplitude of q_{rv}^* and Φ_r^*.

4.2.3. Effect of the wall thickness

To examine the effect of the wall thickness e, the numerical solutions were obtained for $e = 0.02$ to 0.12,

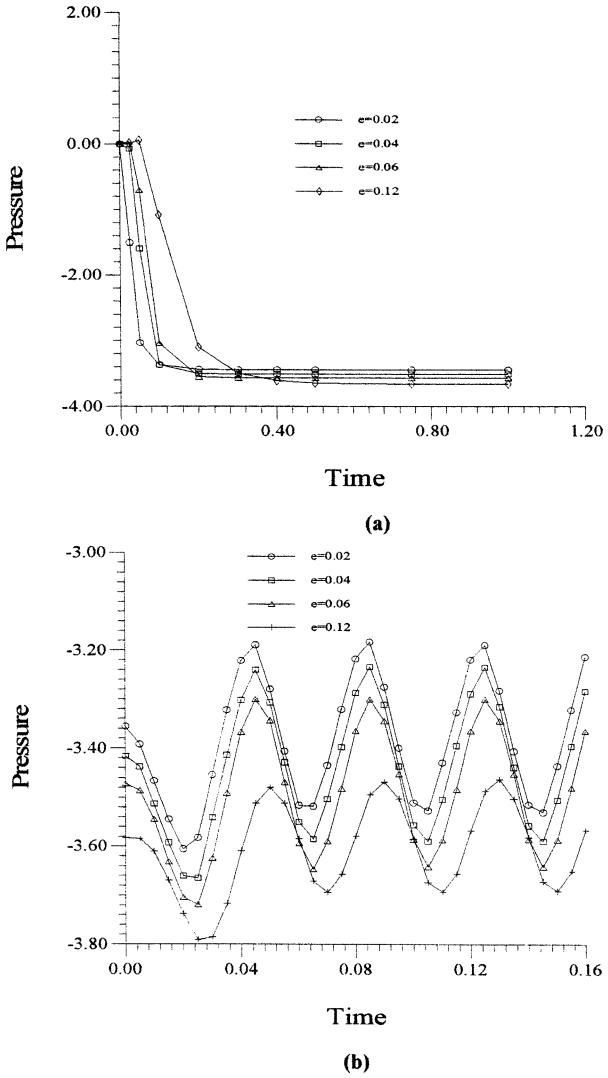

Figure 22. Time-variations of pressure for $r = 0.57$, $z = 0.79$, $R_d = 1$ and for different values of e and (a) a constant heat flux and (b) a periodical heat flux ($Fr = 25$).

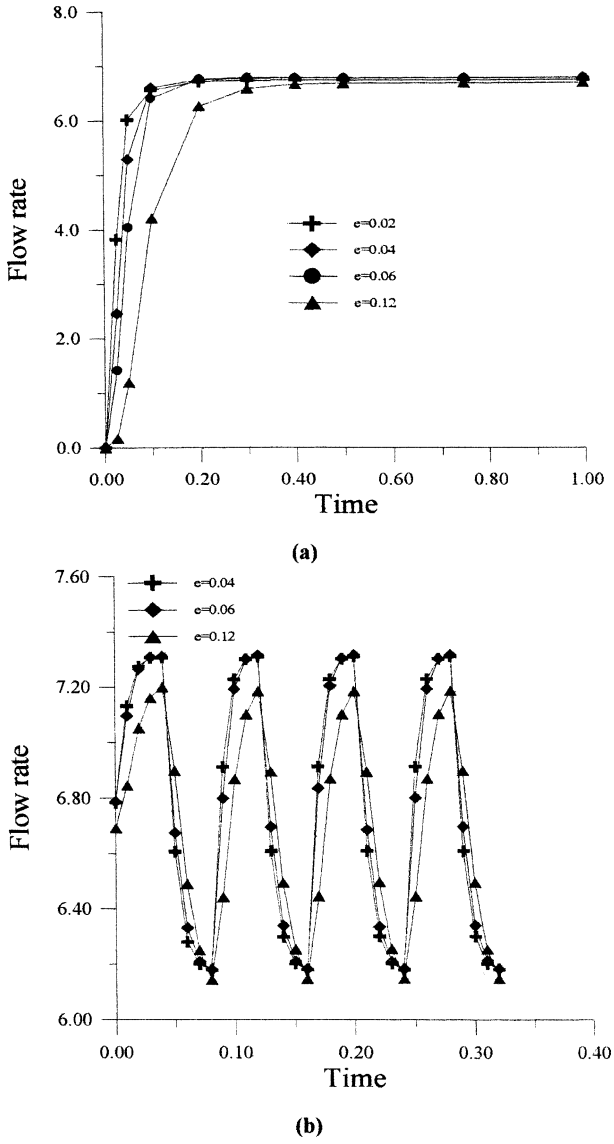

Figure 23. Time-variations of q_v^* for (a) a constant heat flux and (b) a periodical heat flux, for $R_d = 1$ and for different wall thickness.

for $Ra^* = 2{\cdot}10^3$, $A_i = 1$, $r = 0.8$, $z = 0.58$, $Fr = 25$, $R_d = 1$. The two different cases (a constant heat flux at the wall and a periodical heat flux at the wall) are also considered in this section.

In the case of constant wall heat flux, the temperature is found to be increased at first with a decrease in the wall thickness values. In the steady state regime, the temperature at the wall decreases at the inlet and the outlet regions of the medium as the wall thickness is increased (*figure 19*). This is obvious because the increase of the wall thickness will lead, at both edges of the cylindrical enclosure, to an increase in the heat flux loss with the surrounding. Far from the heated wall (*figure 20*), the thermal behaviour is identical, in the unsteady regime, to that corresponding to $r = 1$. There is a difference only in the steady state regime when the temperature far from the heated wall, seems not to be sensitive to any change of the wall thickness.

Figures 21(a) and *22(a)* show that in the case of constant wall heat flux, the steady state regime for pressure and temperature is reached as rapidly as the wall is thin.

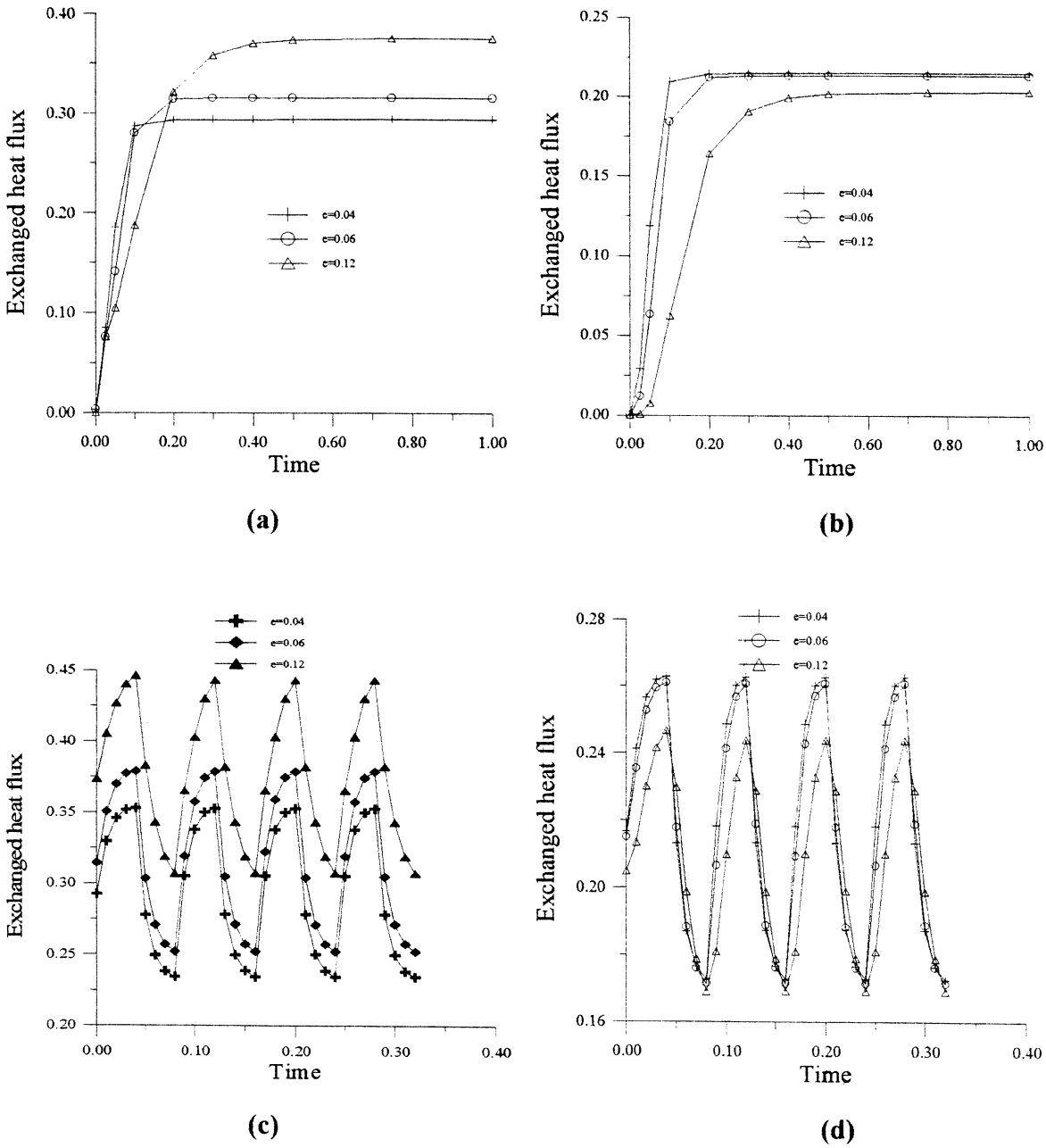

Figure 24. Effect of wall thickness on time-evolution of Φ^* for $R_d = 1$ in the case of (a, b) a constant heat flux and (c, d) a periodical heat flux.

Figures 21(b) and *22(b)* show that the amplitudes of time-variations of the temperature and pressure increase as the wall thickness decreases. This is evident because a thin wall exerts less resistance on heat transfer and then the heat flux fluctuations will be easily transmitted to the interior of the medium.

As indicated by *figure 23*, considering a thick wall will result in a decrease in the flow rate leaving the upper porous surface, and this result occurs in both cases (constant and periodical heat flux density). As expected, the augmentation of the wall thickness will lead to an increase of the exchanged heat flux at the cylinder exit

(*figures 24(a, c)*). If the heat exchange between the heated wall and the surrounding at the exit is not taken into account, an increase of wall thickness values will lead to a decrease in the values of Φ^* (*figures 24(b, d)*).

5. CONCLUSION

The problem of unsteady natural convection which occurs in a vertical cylindrical enclosure opened at both ends, filled with a fluid saturated porous medium, heated with a periodical lateral heat flux density, was the focus of the present investigation. The wall heat conduction is taken into account.

The main results obtained from the numerical solutions can be summarised as follows:

(1) The amplitude of time-variations of pressure and temperature increase as the ratio of thermal diffusivity increases and as the frequency and the wall thickness decrease.

(2) The amplitude of time-variations of the flow rate and the heat flux exchanged at the exit increase when the frequency and the thermal diffusivity ratio decrease.

(3) An increase of the wall thickness provokes an increase in the amplitude of time-variations of the exchanged heat flux and a decrease of the time-variations of the flow rate leaving the upper porous surface of the medium.

REFERENCES

[1] Vafai K., Ettefagh J., The effects of sharp corners on bouyancy driven flows with particular emphasis on outher boundaries, Int. J. Heat Mass Tran. 33 (1990) 2311–2328.

[2] Vafai K., Ettefagh J., Thermal and fluid flow instabilities in buoyancy-driven flows in open ended cavities, Int. J. Heat Mass Tran. 33 (1990) 2329–2344.

[3] Desai C.P., Vafai K., Experimental and numerical study of buoyancy-induced flow and heat transfer in an open annular cavity, Int. J. Heat Mass Tran. 39 (1996) 2053–2066.

[4] Poulikakos D., Bejan A., Unsteady natural convection in a porous layer, Phys. Fluids 26 (1983) 1183–1191.

[5] Poulikakos D., Bejan A., The departure from Darcy flow in natural convection in a vertical layer, Phys. Fluids 28 (1985) 3477–3484.

[6] Yang H.Q., Yang K.T., Xia Q., Periodic laminar convection in a tall vertical cavity, Int. J. Heat Mass Tran. 32 (1989) 2199–2207.

[7] Antohe B.V., Lage J.L., A dynamic thermal insulator: inducing resonance within a fluid saturated porous medium enclosure heated periodically from the side, Int. J. Heat Mass Tran. 37 (1994) 771–782.

[8] Bejan A., Anderson R., Heat transfer across a vertical impermeable partition imbedded in porous medium, Int. J. Heat Mass Tran. 24 (1981) 1237–1245.

[9] Kim D.M., Viskanta R., Study of the effects of conductance on natural convection in differently oriented square cavities, J. Fluid Mechanics 144 (1984) 153–176.

[10] Chang W.J., Lin H.C., Natural convection in a finite wall rectangular cavity filled with an anisotropic porous medium, Int. J. Heat Mass Tran. 37 (1994) 303–312.

[11] Patankar S.V., Numerical Heat Transfer Fluid Flow, Hemisphere/Mc Graw-Hill, New York, 1980.

[12] Vafai K., Convective flow and heat transfer in variable porosity media, J. Fluid Mechanics 147 (1984) 233–259.

[13] Ben Nasrallah S., Amara T., Du Peuty M.A., Convection naturelle instationnaire dans un cylindre rempli de grains ouvert à ses extrémités et dont la paroi est chauffée par un flux de chaleur constant—Validité de l'hypothèse de l'équilibre thermique local, Int. J. Heat Mass Tran. 40 (1997) 1155–1168.

[14] Dalbert A.M., Penot F., Peube J.-L., Convection naturelle laminaire dans un canal vertical chauffé à flux constant, Int. J. Heat Mass Tran. 4 (1981) 1463–1473.

[15] Slimi K., Ben Nasrallah S., Fohr J.P., transient natural convection in saturated porous medium—Validity of Darcy flow model and thermal boundary layer approximations, Int. J. Heat Mass Tran. 41 (1998) 1113–1125.

[16] Hickox C.E., Gartling D.K., A numerical study of natural convection in a vertical, annular, porous layer, in: 21st National Heat Transfer Conf., ASME, 1982, Paper No. 82-HT-68.

[17] Prasad V., Kulacki F.A., Natural convection in a vertical porous annulus, Int. J. Heat Mass Tran. 27 (1984) 207–219.

[18] Prasad V., Natural convection in porous media—An experimental and numerical study for vertical annular and rectangular enclosures, Ph.D. Dissertation, University of Delaware, 1983.

[19] David E., Lauriant G., Prasad V., Non-Darcy natural convection in packed-sphere beds between concentric vertical cylinders, in: Yilmar S.B. (Ed.), AIChE Symp. Ser., Vol. 269 (85), 1989, pp. 90–95.